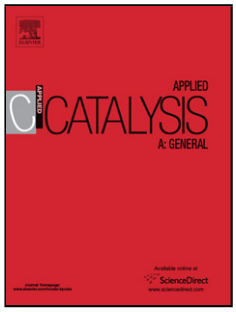

Title: Ferrite catalysts derived from electroplating sludge for high-calorie synthetic natural gas production

Authors: Min Chen, Jizhi Zhou, Jia Zhang, Juan Zhang, Zheng Chen, Jian Ding, Fanhua Kong, Guangren Qian, Jiangang Chen

PII: S0926-860X(17)30040-6
DOI: http://dx.doi.org/doi:10.1016/j.apcata.2017.01.022
Reference: APCATA 16133

To appear in: *Applied Catalysis A: General*

Received date: 26-9-2016
Revised date: 20-1-2017
Accepted date: 26-1-2017

Please cite this article as: Min Chen, Jizhi Zhou, Jia Zhang, Juan Zhang, Zheng Chen, Jian Ding, Fanhua Kong, Guangren Qian, Jiangang Chen, Ferrite catalysts derived from electroplating sludge for high-calorie synthetic natural gas production, Applied Catalysis A, General http://dx.doi.org/10.1016/j.apcata.2017.01.022

Highlights

- Ferrite catalysts were synthesized from electroplating sludge by hydrothermal process.
- Electroplating sludge derived catalyst can produce higher heating value of SNG.
- Electroplating sludge derived catalyst resist thermal shock perfectly.
- Electroplating sludge derived catalyst was more stable and kept intact after reaction.

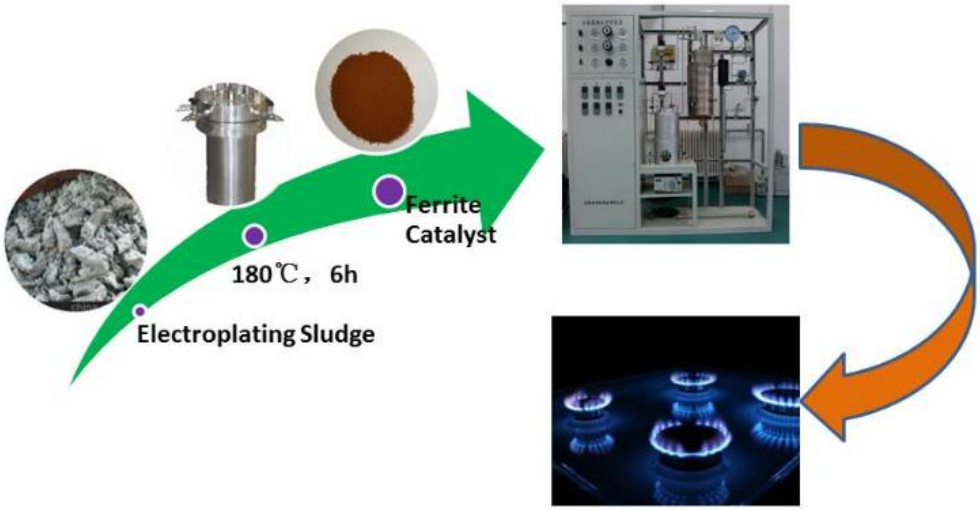

Ferrite catalysts prepared from electroplating sludge are used to produce high-calorie SNG. This method can recycle heavy metals and eliminate the environmental pollution.

Ferrite catalysts derived from electroplating sludge for high-calorie synthetic natural gas production

Min Chen,[a,b] Jizhi Zhou,[a] Jia Zhang,[a] Juan Zhang,[b] Zheng Chen,[b] Jian Ding,[b] Fanhua Kong,[c] Guangren Qian[a*] and Jiangang Chen[b†]

[a] College of Environmental Engineering, Shanghai University, 333 Nanchen Road, Shanghai 200444, PR China.

[b] State Key Laboratory of Coal Conversion, Shanxi Institute of Coal Chemistry, Chinese Academy of Sciences, Taiyuan 030001, Shanxi, PR China.

[c] PetroChina Petrochemical Research Institute, Beijing 100195, PR China.

Abstract

In this study, a ferrite catalyst has been prepared through a facile hydrothermal method using industrial Zn and Fe-rich electroplating sludge as raw materials and utilized for the first time as an efficient catalyst for methanation of syngas. The ferrite catalyst showed pretty good catalytic performance during the stability test at 340 ^{o}C for 300h, meanwhile exhibited a higher resistance to thermal shock (600 ^{o}C for 12 h) than that of the catalyst prepared from pure chemical reagents or commercial methanation catalyst. More importantly, a high-calorie natural gas with heating value of 41.73 MJ·Nm^{-3} could be obtained via methanation of syngas over the ferrite catalyst derived from electroplating sludge. Thus, this work provides some new insights for utlising solid waste as raw material for methanation catalyst, which is very cheap.

Key words； electroplating sludge, ferrite，methanation, high-calorie SNG.

*Corresponding author: E-mail: grqian@shu.edu.cn

†Corresponding author: Email: chenjg@sxicc.ac.cn

1. Introduction

With the development of electroplating industry, sludge generated from wastewater treatment plants increases, especially in the developing countries, such as China, electroplating factories produce approximately 10 million tons of electroplating sludge annually [1]. Since the sludge is enriched in heavy metals such as Ni, Zn, Fe, Cu, Cr and Cd *etc.*, it is hazardous to environment, as toxic metals posing a potential risk to the soil and groundwater. Currently, several methods have being used to dispose the electroplating sludge and the most popular methods are landfill or metal recovery by suitable technologies [2]. Landfill is not environmentally benign and may cause large amount of waste of valuable metals [3], thus, it is very promising to maximize the recovery and reusing of heavy metals economically.

Last decades witness a fairly rapid development of recovery of heavy metals from electroplating sludge, such as ion exchange, leaching-solvent and membrane separation, etc. However, these traditional methods have certain obvious drawbacks, including complicated separation process, high capital cost and relatively low recovery. Recently ferrite inclusion becomes more and more popular as a novel treatment to reuse electroplating sludge. During the process heavy metal ions (Mn^{2+}, Cu^{2+}, Ni^{2+}, Zn^{2+}, Co^{2+}, Fe^{3+}, Al^{3+} or Cr^{3+}) which match well with the ferrite texture can be fixed in the crystal lattice of spinel ferrite [4]. Generally, prepared ferrites are tentatively used as functional materials. Nonetheless, the heavy metals are well known to be the main elements of heterogeneous catalysis. For instance, Ni, Zn, Cr, Mn, *etc.* in ferrite are used as promoters to enhance the efficiency or control the selectivity of hydrocarbon production in CO hydrogenation [5-7].

As is known, natural gas is an excellent energy carrier due to low carbon release, advantageous combustion, the existing pipeline grid for transportation and distribution. It is also used as resources of high purity hydrogen for chemical industry (trace carbon monoxide present in H_2-rich gases) such as NH_3 synthesis and methanol production [8]. In order to extend the application of natural gas as town gas, it is extremely important to improve the heat value. For example, Japan and South Korea

import liquefied natural gas (LNG) with high heating value typically in a range between 41 and 46 $MJ \cdot Nm^{-3}$ [9]. Since Sabatier et al. discovered the hydrogenation of CO to methane, named methanation (Eq. (1)), the technology had been widely developed and applied to produce synthetic natural gas (SNG). However, side reactions water-gas shift (WGS: Eq. (2)) occurs along to certain degree when the syngas is introduced. The stoichiometric ratio of H_2/CO will changed according to the percent of two component reactions.

$$3H_2 + CO \rightarrow CH_4 + H_2O \qquad \Delta H_{298} = -206\ kJ \cdot mol^{-1} \qquad (1)$$

$$CO + H_2O \rightarrow CO_2 + H_2 \qquad \Delta H_{298} = -41.1\ kJ \cdot mol^{-1} \qquad (2)$$

Nonetheless, the selectivity of CH_4 and CO_2 represents the degree of methanation and WGS reaction, respectively. WGS reaction is undesirable in producing high-calorie SNG process, and should be suppressed to reduce the selectivity of CO_2 because higher CO_2 content yields SNG of lower heating value. In consequence, mediate selectivity of CH_4 and C_{2+} hydrocarbons with low CO_2 content is primary. Nickel is the most selective methanation catalyst and displays little activity for WGS reaction [10]. However, Iron catalysts are known to hold high Fischer-Tropsch synthesis activity with a low selectivity towards methane [11]. That is the reason why Ni-Al_2O_3 cannot produce high calorie SNG like Fe contained catalysts. Typical performance of Ni catalyst was reports by Dennis, which presented the highest CO conversion and CH_4 selectivity about 80% and 85% with few CO_2 during the temperature range of 220-380 ^oC [10]. Lee *et al.* reported at 300 ^oC syngas methanation (81.7-98.2% CO conversion) produced the high-calorie SNG which contained 22-33% CO_2, 18-27% CH_4 and 36-40% C_{2-4} by using a series of Fe-Zn catalysts [9].

Using syngas generated from carbon sources (coal, biomass, coke oven gas, municipal solid waste, etc.) to produce SNG has been considered as a promising way towards the sustainable development and clean utilization of coal in China, whose energy consumption has to depend mainly on coal [12]. For instance, the remote coal resource in west of China could be converted into SNG and transported to consumer city in East by ready SNG pipeline. Nowadays the heating value of SNG can

be enhanced by producing additional C_2-C_4 hydrocarbons whose heating value exceed about 40 MJ·Nm^{-3}(i.e. CH_4: 37.85 MJ·Nm^{-3}; C_2H_6: 67.33 MJ·Nm^{-3}; C_2H_4: 61.42 MJ·Nm^{-3}; C_3H_8: 97.19 MJ·Nm^{-3}; C_3H_6: 90.61 MJ·Nm^{-3}; n-C_4H_{10}: 128.68 MJ·Nm^{-3}; C_4H_8: 121.69 MJ·Nm^{-3}) during methanation [9, 13, 14]. The most popular methanation catalyst is Ni supported on Al_2O_3. However, it yields less ethane or propylene. Among the various catalysts in CO hydrogenation, Fe is reported to produce light paraffin as most efficiently catalyst and Zn is always used to improve the selectivity of paraffin [15-17]. Besides, Mn as promoter can also enhance the yield of C_2-C_4 and decrease the selectivity of methane [14]. Since diversify metal ions exist in ferrite prepared from electroplating sludge, it is anticipated that the ferrite might produce more C_{2+} hydrocarbons and then high-calorie SNG. Moreover, the spinel structure might be more stable on condition of heat shock in methanation reactor, which is critical to operate stably [18].

In this work, ferrite catalyst prepared from electroplating sludge (catalyst A) was tested in a methanation reaction in a fixed bed reactor to produce high-calorie SNG. For purpose of comparison, Ni-Zn ferrite (catalyst B) made by pure chemical reagents and industrial catalyst Ni-Al_2O_3 (catalyst C) were also evaluated by methanation reaction. Catalytic performance of these catalysts for syngas methanation at different temperature was studied. Besides, catalytic performance was also retested after high temperature processing. Results showed that catalyst A exhibited good activities to produce high-calorie SNG. Meanwhile, this catalyst could suppress water gas shift reaction significantly. What is more, it showed the slightest drop of activity upon the heat-treatment.

2. Experimental section

2.1 Catalyst preparation

Electroplating sludge, which were directly collected from Taizhou electroplating company, Zhejiang province, China, S1 (Zn-rich) and S2 (Fe-rich) contained 80.78 and 56.12 wt% of water, respectively. The electroplating wastewater of S1 and S2 were separately collected from two workshops (S1 : corrosion protection by Zn of an object; S2 : pickling). The transformantion of the electroplating waste water into

electroplating sludge follow the treatment process shown in Fig. 1. As listed in Table 1, the main heavy metal elements were Zn (22.2 wt%) and Fe (23.9 wt%). The chemical reagents, such as $Fe(NO_3)_3 \cdot 9H_2O$, $Zn(NO_3)_2 \cdot 6H_2O$, $Ni(NO_3)_2 \cdot 6H_2O$, NaOH, HNO_3 were all of analytical grade and purchased from Sino pharm Group Chemical Reagent Co. Ltd., China. Industrial catalyst J101 was purchased from Nanjing Chemical Catalyst factory.

2.2 Ferrite preparation via hydrothermal treatment

Catalyst A was prepared by hydrothermal method in typical synthesis using electroplating sludge. In the first step, electroplating sludge from S1 (7.9g) and S2 (5g) were dissolved in a solution of deionized water (300.0 mL) to form heterogeneous slurry by stirring in a 500 mL high-pressure autoclave. The amount of Iron additive (iron scrap) was determined by stoichiometric formula of ferrite and the sludge composition. NaOH was used to keep the pH of reaction mixture at 9.0~9.5. Next, the autoclave was heated at 180 ^{o}C for 6 h. Resulting precipitate was collected by centrifugation, washed with distilled water to remove any impurities and dried at 105 ^{o}C for 15 h after the autoclave cooled to room temperature. At last, the catalysts were calcined at 950 ^{o}C for 4 h in muffle. The simulation catalyst B was prepared by chemical regent using $Fe(NO_3)_3 \cdot 9H_2O$, $Zn(NO_3)_2 \cdot 6H_2O$ and $Ni(NO_3)_2 \cdot 6H_2O$ in the same process as catalyst A. Catalyst C J101 was purchased from Nanjing Chemical Catalyst factory. The catalyst B and C were designated to make comparisons with catalyst A in the methanation reaction.

2.3 Characterization

X-ray diffractometer was employed to analyze the XRD profiles of as-obtained ferrites and spent catalysts. The XRD patterns were acquired on a DX-2700 diffractometer with monochromatic Cu Kα radiation (λ = 0.15418nm) operating at 40 kV and 30 mA at a scanning speed of 4°·min^{-1} in 2θ = 5-80°. The metal compositions in sludge and as-obtained ferrites were determined by inductively coupled plasma optical emission spectrometer (ICP-OES, Optima2100DV, PerkinElmer) after the suitable treatment. Temperature-programmed reduction (TPR) was carried out in a quartz tube reactor loaded with about 20 mg of freshly calcined powder catalyst by

glass wool to study the reducibility of the catalysts. Silica gel desiccant and 5A molecular sieve were applied to purify effluent. The TPR experiments were performed in a mixture gas of 5% H_2/N_2 at flow rate of 50 mL·min^{-1}. The quartz tube reactor was heated at a linear programmed rate of 10 °C·min^{-1} from room temperature to 1000 °C and the consumption of H_2 in the process of TPR was monitored by comparison of the thermal conductivity difference between the reference and the product gas. Nitrogen physisorption isotherms were obtained with a Micromeritics TriStar II 3020 instrument to measure BET surface area, pore volume and average pore diameter of the fresh catalysts. Prior to analysis, each sample was outgassed at room temperature for 24 h to remove the moisture and other adsorbates. The morphology of as synthesized samples was monitored by using scanning electron microscope (SEM, Zeiss Supra 55). Temperature programmed oxidation (TPO) measurements was carried out on a 2 mm (I.D.) quartz tube. 30 mg of used catalysts were placed between two quartz wool plugs and heated from ambient temperature to 1000 ^{o}C at 10 ^{o}C·min^{-1} under 10% O_2/He stream. Produced carbon dioxide was measured on-line by the GC. Furthermore, for comparison purposes, mechanical mixture of 5mg carbon and 25mg fresh catalyst A was also tested as reference material.

2.4 Catalyst testing

Methanation reaction was carried out in a 1.2 cm (O.D.) stainless steel fixed-bed. In a typical run, catalysts with grain size ranging in 60−80 mesh were placed between three layers of quartz sands in the bed. In order to facilitate the heat transfer and prevent hot spots resulting from the exothermal character of the reaction, the calcined 1.0 mL catalysts (1.2g of catalyst A) were diluted with 1 mL quartz sands in the same size. Bed temperature controlled by a temperature controller was monitored axially using a type-K movable thermocouple which was buried in the catalytic bed. Before the reaction, catalysts were activated on-line in a stream of hydrogen at 400 ^{o}C for 6h at atmospheric pressure with a heating rate of 1 °C·min^{-1}. Then the pressure was elevated to 2.0 MPa by feeding the syngas mixture (H_2/CO = 2) from the pressurized manifold via individual mass flow controller. The gas hourly

space velocity (GHSV) was set at 3000 h^{-1}. Subsequently, it was heated to the desired reaction temperature by steps of 1 °C·min^{-1}. Catalyst samples were activated in synthesis gas at 2 MPa by increasing the temperature from 280 ^{o}C to 360 °C. Catalytic performance and thermostability were further investigated after high-temperature treatment processing (that is, 600 ^{o}C for 12 h). Heavy hydrocarbons were collected by a heated trap (at 130 °C and reactor pressure) placed immediately below the reactor. Products like water and oil were collected by a cold trap placed after the heated trap. The tail gas and reactant were analyzed on line by gas chromatographs (Shanghai Haixin GC-950) equipped with a thermal conductivity detector and a flame ionization detector. And the gas chromatographs worked with a packed column (TDX-101) filled with carbon molecular sieve. Quantitatively of products were determined by calibrated area normalization; accordingly, the CO conversion and product selectivity were calculated on the basis of the equations.

3. Result and discussion

3.1 X-Ray diffraction (XRD)

Fig. 2a and b showed the XRD patterns of the fresh catalysts. As seen in Fig. 2a, the peaks at 18.5°, 30.3°, 35.7°, 43.3°, 53.7°, 57.1°, 62.7° and 74.2° of ferrite were apparent in catalyst A though a few peaks ascribed to impurity were also exist. Most importantly, these typical diffraction peaks of ferrite matched well with (Ni, Zn)Fe_2O_4 (PDF 08-0234) [19], which indicated that ferrite with the spinel structure was successfully synthesized from sludge by the hydrothermal method [20, 21]. The impurity peaks (Fig. 2a) at the value of 2θ equal to 18.6°, 30.7°, 36.1°, 37.8°, 43.9°, 54.5°, 58.1° and 63.8° were assigned to another form of Fe_2SiO_4 phase (PDF 44-1385). All peaks (Fig. 2b) observed at 18.3^{o}, 30.1^{o}, 35.4^{o}, 43.0^{o}, 53.4^{o}, 56.9^{o}, 62.5^{o}, and 74.0^{o} could be corresponded to (Ni, Zn)Fe_2O_4 suggesting that the ferrite from reagent was pure phase.

In order to figure out the phase transformations after the methanation reaction, the XRD patterns of the used catalysts were depicted in Fig. 2. Fig. 2c showed spent catalyst A almost maintained the spinel feature, which still matched well with (Ni, Zn)Fe_2O_4 and Fe_2SiO_4 after the whole reaction [22-24]. For the spent catalyst B, the

most intense reflections at 2θ of 35.5°, 40.0°, 42.6°, and 45.0° (Fig. 2d) represented the characteristic peaks of Fe_5C_2 (PDF 20-0508) which was known as catalytically active phase for Fischer-Tropsch synthesis [25]. Additionally, peaks corresponding to ZnO and Ni were observed in Fig. 2d. This result meant that the spinel phase in catalyst B was not so stable as that in catalyst A. This difference might be due to the impurity elements in sludge. For instance, addition of silica could enhance the stability of iron-based catalyst during Fischer–Tropsch synthesis [26-30]. Though the formation of Fe_2SiO_4 inhibited the reduction of iron oxide or carburization of catalysts, it increased the selectivity of light hydrocarbon [31, 32].

Lee et al. reported that $ZnFe_2O_4$ could inhibit sintering of catalyst A during methanation reaction and thermal treatment [33]. Mn could improve the surface acidity and enhance carbon-rich environment on the surface of the catalyst A, which leaded to the increase of the selectivity of C_2-C_4 [14]. By providing H_2 dissociation sites, Cu increased the reduction ability of Fe_2O_3 to Fe_3O_4 and the rate of carburization. Thus, the content of CH_4 and paraffin increased in FTS products [33, 34]. With above knowledge, promoting elements such as Zn, Mn, Cu, etc. in sludge were likely to produce the higher heating-value SNG and make catalyst more stable. They might affect the FTS performance individually or jointly [34]. Therefore the effect of catalyst A was a composite promotion and further study is essential to confirm the influence of individual element.

3.2 Inductively coupled plasma optical emission spectrometer (ICP-OES)

The mass fractions of different elements in catalysts were analyzed using ICP-OES. Table 2 showed that the contents of Zn and Ni were almost the same in catalyst A and B. The several extra elements such as Cu, Al, Cr, and Mn in catalyst A might as structural promoter to promote the reaction of methanation. Catalyst C was consisted of Ni and Al, with the content of 21.0 % and 23.30 %, respectively. Since Ni supported on Al_2O_3 was a typically methanation catalyst we speculated that catalyst C would show highest selectivity of methane.

3.3 Temperature-programmed reduction (TPR)

The TPR characterization was used to obtain information about the reduction

behavior of catalysts (Fig. 3). Fig. 3a showed a small H_2 consumption peak in the range of 290-310 ^oC which might be assigned to be the reduction of CuO to Cu. Then the second one at about 335 ^oC was related to the reduction of Ni^{2+} to Ni. The third peak appeared in a wide range of 400-550 ^oC was ascribed to the reduction of Fe_2O_3 to Fe_3O_4. The forth broad peak observed in range of 550-770 ^oC was associated with Fe_3O_4 to FeO and the last higher than 850 ^oC was due to conversion of FeO to Fe [35, 36]. Fig. 3b showed a characteristic curve with four peaks of catalyst B in the H_2-TPR spectra. The first hydrogen consumption weak peak was attributed to the conversion of Ni^{2+} to Ni. The following peaks which appeared at about 375, 400, 500 and 700 ^oC could be assigned to the following consecutive reduction of the catalyst B: Fe_2O_3 → Fe_3O_4 → FeO → Fe. A similar tendency was also discovered for the nickel ferrite catalyst by Löfberg et al. [35]. In Fig. 3c, the higher and broader small shoulder at about 400 ^oC was attributed to reduction of bulk nickel oxide [37].

These observations suggested that the reduction of Fe_2O_3 in catalyst B was easier than catalyst A. That was, the presence of Fe_2SiO_4 which led to the Fe_2O_3 reduction more difficult [18]. The results were in agreement with the conclusion from the X-Ray diffraction. Catalyst C showed the lowest temperature of the reduction of NiO. The facilitated reduction of NiO in catalyst C was attributed to its supporting structure.

3.4 N_2-adsorption-desorption measurements

Catalyst nanoparticles were analyzed by Brunauer–Emmett–Teller (BET) measurement. The BET surface area value of the catalyst A calculated from N_2 isotherms was 12.9 $m^2 \cdot g^{-1}$, however, catalyst B was 5.8 $m^2 \cdot g^{-1}$. Obviously, catalyst A was about 2 times that of catalyst B. It had been reported that the BET surface area of the iron catalysts could be increased by silica incorporation [28, 30]. Besides, the elevated surface area of catalyst A could be partially contributed to some impurity phase (Fe_2SiO_4) in XRD [38].

Nitrogen-desorption-adsorption isotherms described the textural analyses of the catalysts in Fig. S1. According to IUPAC classification, all N_2 isotherms were type IV. The pores had uniform size with an evident hysteresis H3 loop in the 0.8–1.0

range of relative pressure, clearly related to nitrogen capillary condensation. These indicated that catalysts were characteristic of mesoporous materials with regard to mean pore-size distribution (Fig. S2).

3.5 Temperature programmed oxidation (TPO)

TPO analysis was performed on the used catalysts to measure carbon deposition. For purpose of quantification comparison, carbon black was used as standard substance. The spent catalyst A, B or reference material were carried out at the same heating rate of 10 $^{o}C \cdot min^{-1}$. Fig. 4 showed that much lower amount of carbon was deposited on catalyst A than that of B. Furthermore, several CO_2 peaks were observed, indicating different types of carbons with different reactivity toward oxidation [39-40]. Besides, the peak maximum of carbon species in ferrite catalysts was shifted to lower temperature compared with reference material, indicating that the deposited carbon species were mainly oxidized by lattice or surface oxygen [41]. Thus, the TPO profile of spent catalysts suggesting catalyst A held good carbon resistance than that of catalyst B.

3.6 Catalytic activity

It could be seen from Fig. 5 that conversion of CO increased with the rising of temperature on these catalysts. The conversion of CO for catalyst B was the highest during the whole reaction processing. Besides, the conversion of CO for catalyst A was larger than that of catalyst C, except below 300 ^{o}C. In other words, the catalyst A showed better performance than commercial catalyst at higher temperature. At 360 ^{o}C, catalyst A, B and C showed the highest conversion of CO, which were 87.0 %, 94.6 % and 39.9%, respectively.

Fig. 6 showed that the selectivity of CH_4 for catalyst A was 70.1 % at 280 ^{o}C, furthermore it reached up to the maximum (72.8 %) when the temperature was 300 ^{o}C. However, the catalyst B and C exhibited the highest selectivity of CH_4 at 320 ^{o}C. The selectivity of CH_4 for catalyst C was larger than that of catalyst A above 300 ^{o}C. Catalyst B showed the lowest selectivity of CH_4 on the whole. The different CO_2 selectivity against temperature was shown in Fig.7. As a result, the ferrite catalyst prepared from pure regents showed high CO_2 selectivity, while the Ni-Al_2O_3 catalyst

showed much less CO_2 selectivity. The predominent cause of the phenomenon was that Ni catalysts were more favorable for the methanation than the WGS reaction under high reaction pressure [42]. Surprisingly, the selectivity of CO_2 for catalyst A was as low as catalyst C. The low CO_2 selectivity in catalyst A might be correlated with the heavy metal modification which leaded to different reducibility and carburation ability.

On the whole, catalyst A showed the higher CH_4 selectivity, higher C_{2-4} selectivity and lower CO_2 selectivity than that of catalyst B and C. It could be elucidated that catalyst A could be used to produce higher heating value SNG with appropriate temperature.

To investigate the thermal stability of the catalysts, high temperature treatment was performed and catalytic activity was tested before and after that. As shown in Fig. 8 CO conversion of catalyst A decreased from 87.0 % to 57.6 % after heat treatment, whereas that of catalyst B and C decreased from 94.6 % to 30.7 % and 39.9 % to 6.0 %, respectively. Both A and B exhibited higher catalytic reactivity after high-temperature processing in contrast to catalyst C. The good resistance to thermal shock of catalyst A and B might be due to spinel structure. Besides, the reason why catalyst A showed the best resistance to thermal shock might be explained as the heavy metal promotion, by which the spent catalyst A was dense, whereas catalyst B occurred coagulations on the surface as shown in SEM (Fig. S3c-d). Such a privilege is of great importance in the notorious strong exothermic reaction. A completely engineering importance of it in methanation reaction was worth of further study.

Heating value ($\frac{MJ}{Nm3}$)= $\sum_{i=1}^{4}\{\frac{volume\ fraction*heat\ of\ combustion(\frac{MJ}{mol})}{specific\ volume\ (\frac{Nm3}{mol})}\}$ of hydrocarbon of carbon number (3)

The SNG calorie produced from catalyst A, B and C was calculated (according to Eq. (3) and table 3), with the highest heating value of 41.7 (340 ^{o}C) MJ·Nm^{-3}, 32.3 (320 ^{o}C) MJ·Nm^{-3} and 36.0 (320 ^{o}C) MJ·Nm^{-3}, respectively. The highest heating value of catalyst A was ascribed to mediate CO_2 content and C_{2+} hydrocarbons content. Besides, catalyst C produced the least by-product comparing catalyst A and B. Thus,

the reason why catalyst A could produce high-calorie SNG and catalyst C always used in methanation were obviously.

3.7 Stability

In order to investigate the stability of catalyst A, a long-term test was performed under 340 ^{o}C, 2 MPa up to 300 h. Fig. 9 showed the catalytic stability of catalyst A during methanation process. In the 300 h stability test, the CO conversion, CH_4 and CO_2 selectivity obtained on catalyst A maintained at about 65%, 50% and 13%, respectively. No deactivation was observed in the time on stream, suggesting an excellent catalytic stability of the catalyst prepared from electroplating sludge. Here, the resistance to deactivation might be ascribed to the presence of heavy metals.

3.8 Economic assessment

The catalyst cost was evaluated for next step of application. Dealing electroplating sludge would spend 149.81-299.63 $\$\cdot t^{-1}$ nowadays. In other words, producing catalyst A not only could ignore the cost of raw materials but also saved the handling expense and offer environmental benefits. So, the feedstock of catalyst A was assumed to be -224.72 $\$\cdot t^{-1}$.

During hydrothermal processing, the electricity consumption was approximately 200 kw·h. The cost of desalted water was calculated at 2.55 $\$\cdot t^{-1}$ and electricity was 0.12 $/kw·h.

Table 4 showed among the three catalysts, catalyst C was the most expensive one which was almost 33 times than that of catalyst A. Catalyst B involved slightly higher cost because of the use of pure chemicals regents, while catalyst A resulted in most cost-saving because of the reuse of the electroplating sludge.

4. Conclusions

Ferrite catalysts were synthesized by facilitating waste material, *i.e.*, electroplating sludge. Our study demonstrated that the sludge could be used as a valuable resource for synthesizing a highly active and stable methanation catalyst. Comparing with catalyst B prepared by pure reagents and catalyst C employed in industry, electroplating sludge derived catalyst could produce higher heating value of SNG, resist thermal shock perfectly and suppress water gas shift efficiently. Besides,

due to the presence of impurity elements catalyst A was more stable and kept intact after reaction. In a word, a new promising route to handle electroplating sludge and synthesis catalyst is provided by this work.

Acknowledgements

Financial support is acknowledged from the Natural Science Foundation of China (Grant No. 21673272, 21373254) and PetroChina (Project No. 14-08-05-02). We would like to thank Mr. Wenbin Zhang and Mr. Lei Xie for the facilitation in the equipment maintenance, Mrs. Yingying Xue, Mr. Yongbiao Zhai, Mr. Yanting Liu and Mr. Buhuan Wang for the helpful discussions.

Notes and references

[1] J. Zhang, J. Zhang, Y. Xu, H. Su, X. Li, J.Z. Zhou, G. Qian, L. Li, Z.P. Xu, Efficient selective catalytic reduction of NO by novel carbon-doped metal catalysts made from electroplating sludge, Environ. Sci. Technol. 48 (2014) 11497-11503.

[2] M. Arsenovic, Z. Radojevic, S. Stankovic, Removal of toxic metals from industrial sludge by fixing in brick structure, Constr Build Mater 37 (2012) 7-14.

[3] N. Nagarajan, P. Gunasekaran, P. Rajendran, Genetic characterization, nickel tolerance, biosorption, kinetics, and uptake mechanism of a bacterium isolated from electroplating industrial effluent, Can. J. Microbiol. 61 (2015) 297-306.

[4] D. Chen, J. Hou, L.-h. Yao, H.-m. Jin, G.-R. Qian, Z.P. Xu, Ferrite materials prepared from two industrial wastes: Electroplating sludge and spent pickle liquor, Sep. Purif. Technol. 75 (2010) 210-217.

[5] V.R.R. Pendyala, G. Jacobs, M.K. Gnanamani, Y. Hu, A. MacLennan, B.H. Davis, Selectivity control of Cu promoted iron-based Fischer-Tropsch catalyst by tuning the oxidation state of Cu to mimic K, Appl. Catal. A: Gen. 495 (2015) 45-53.

[6] M. Al-Dossary, A.A. Ismail, J.L.G. Fierro, H. Bouzid, S.A. Al-Sayari, Effect of Mn loading onto MnFeO nanocomposites for the CO_2 hydrogenation reaction, Appl. Catal. B: Environ. 165 (2015) 651-660.

[7] H. Wang, Y. Yang, J. Xu, H. Wang, M. Ding, Y. Li, Study of bimetallic interactions and promoter effects of FeZn, FeMn and FeCr Fischer–Tropsch synthesis catalysts, J. Mol. Catal. A: Chem. 326 (2010) 29-40.

[8] J. Gao, Q. Liu, F. Gu, B. Liu, Z. Zhong, F. Su, Recent advances in methanation catalysts for the production of synthetic natural gas, RSC Adv. 5 (2015) 22759-22776.

[9] Y.H. Lee, D.-W. Lee, H. Kim, H.S. Choi, K.-Y. Lee, Fe–Zn catalysts for the production of high-calorie synthetic natural gas, Fuel 159 (2015) 259-268.

[10] C. Cheng, D. Shen, R. Xiao, C. Wu, Methanation of syngas (H_2/CO) over the different Ni-based catalysts, Fuel 189 (2017) 419-427.

[11] C.G. Visconti, M. Martinelli, L. Falbo, A. Infantes-Molina, L. Lietti, P. Forzatti, G.

Iaquaniello, E. Palo, B. Picutti, F. Brignoli, CO_2 hydrogenation to lower olefins on a high surface area K-promoted bulk Fe-catalyst, Appl. Catal. B: Environ. 200 (2017) 530-542.

[12] Y. Li, Q. Zhang, R. Chai, G. Zhao, Y. Liu, Y. Lu, Structured Ni-CeO_2-Al_2O_3/Ni-Foam Catalyst with Enhanced Heat Transfer for Substitute Natural Gas Production by Syngas Methanation, ChemCatChem 7 (2015) 1427-1431.

[13] T. Inui, A. Sakamoto, T. Takeguchi, Y. Ishigaki, Synthesis of Highly Calorific Gaseous Fuel from Syngas on Cobalt-Manganese-Ruthenium Composite Catalysts, Ind. Eng. Chem. Res. 28 (1989) 427-431.

[14] Y.H. Lee, H. Kim, H.S. Choi, D.-W. Lee, K.-Y. Lee, Co-Mn-Ru/Al_2O_3 catalyst for the production of high-calorific synthetic natural gas, Korean J. Chem. Eng. 32 (2015) 2220-2226.

[15] H.M.T. Galvis, J.H. Bitter, C.B. Khare, M. Ruitenbeek, A.I. Dugulan, K.P.d. Jong, Supported Iron Nanoparticles as Catalysts for Sustainable Production of Lower Olefins, Science 335 (2012) 835-838.

[16] S.L. Soled, E. Iglesia, S. Miseo, B. DeRites, R. Fiato, Selective synthesis of α-olefins on Fe-Zn Fischer-Tropsch catalysts, Top. Catal. (1995) 193-205.

[17] S. Li, A. Li, S. Krishnamoorthy, E. Iglesia, Effects of Zn, Cu, and K promoters on the structure and on the reduction, carburization, and catalytic behavior of iron-based Fischer–Tropsch synthesis catalysts, Catal. Lett. 77 (2001) 197-205.

[18] P. Liu, H. He, G. Wei, X. Liang, F. Qi, F. Tan, W. Tan, J. Zhu, R. Zhu, Effect of Mn substitution on the promoted formaldehyde oxidation over spinel ferrite: Catalyst characterization, performance and reaction mechanism, Appl. Catal., B 182 (2016) 476-484.

[19] Y. Wang, X. Wu, W. Zhang, W. Chen, Synthesis and electromagnetic properties of La-doped Ni–Zn ferrites, J. Magn. Magn. Mater. 398 (2016) 90-95.

[20] K.E. deKrafft, C. Wang, W. Lin, Metal-Organic Framework Templated Synthesis of Fe_2O_3/TiO_2 Nanocomposite for Hydrogen Production, Adv. Mater. 24 (2012) 2014-2018.

[21] A.M. Afzal, M. Umair, G. Dastgeer, M. Rizwan, M.Z. Yaqoob, R. Rashid, H.S. Munir,

Effect of O-vacancies on magnetic properties of bismuth ferrite nanoparticles by solution evaporation method, J. Magn. Magn. Mater. 399 (2016) 77-80.

[22] A. Hajalilou, S.A. Mazlan, K. Shameli, A comparative study of different concentrations of pure Zn powder effects on synthesis, structure, magnetic and microwave-absorbing properties in mechanically-alloyed Ni–Zn ferrite, J. Phys. Chem. Solids 96-97 (2016) 49-59.

[23] A. Boudjemaa, I. Popescu, T. Juzsakova, M. Kebir, N. Helaili, K. Bachari, I.-C. Marcu, M-substituted (M = Co, Ni and Cu) zinc ferrite photo-catalysts for hydrogen production by water photo-reduction, Int. J. Hydrogen Energy 41 (2016) 11108-11118.

[24] N. Kavitha, P. Manohar, Magnetic and Electrical Properties of Magnesium-Substituted Ni–Zn Ferrites, J Supercond Nov Magn 29 (2016) 2151-2157.

[25] W. Chen, Z. Fan, X. Pan, X. Bao, Effect of Confinement in Carbon Nanotubes on the Activity, J. Am. Chem. Soc. 130 (2008) 9414-9419.

[26] C.-H. Zhang, H.-J. Wan, Y. Yang, H.-W. Xiang, Y.-W. Li, Study on the iron–silica interaction of a co–precipitated Fe/SiO_2 Fischer–Tropsch synthesis catalyst, Catal. Commun. 7 (2006) 733-738.

[27] K. Jothimurugesan, J.G. Goodwin Jr, S.K. Gangwal, J.J. Spivey, Development of Fe Fischer-Tropsch catalysts for slurry bubble column reactors, Catal. Today 58 (2000) 335–344.

[28] H. Suo, S. Wang, C. Zhang, J. Xu, B. Wu, Y. Yang, H. Xiang, Y.-W. Li, Chemical and structural effects of silica in iron-based Fischer–Tropsch synthesis catalysts, J. Catal. 286 (2012) 111-123.

[29] M. Qing, Y. Yang, B. Wu, J. Xu, C. Zhang, P. Gao, Y. Li, Modification of Fe–SiO_2 interaction with zirconia for iron-based Fischer–Tropsch catalysts, J. Catal. 279 (2011) 111-122.

[30] R.P. Mogorosi, N. Fischer, M. Claeys, E. van Steen, Strong–metal–support interaction by molecular design: Fe–silicate interactions in Fischer–Tropsch catalysts, J. Catal. 289 (2012) 140-150.

[31] D.B. Bukur, X. Lang, D. Mukesh, W.H. Zimmerman, M.P. Rosynek, C. Li, Binder/Support Effects on the Activity and Selectivity of Iron Catalysts in the Fischer-Tropsch Synthesis, Ind. Eng. Chem. Res. 29 (1990) 1588-1599.

[32] H. Suo, C. Zhang, B. Wu, J. Xu, Y. Yang, H. Xiang, Y. Li, A comparative study of Fe/SiO_2 Fischer–Tropsch synthesis catalysts using tetraethoxysilane and acidic silica sol as silica sources, Catal. Today 183 (2012) 88-95.

[33] S. Li, A. Li, S. Krishnamoorthy, E. Iglesia, Effects of Zn, Cu, and K promoters on the structure and on the reduction, carburization, and catalytic behavior of iron-based Fischer-Tropsch synthesis catalysts, Catal. Lett. 77 (2001) 197-205.

[34] C. Zhang, Y. Yang, B. Teng, T. Li, H. Zheng, H. Xiang, Y. Li, Study of an iron-manganese Fischer–Tropsch synthesis catalyst promoted with copper, J. Catal. 237 (2006) 405-415.

[35] R. Benrabaa, A. Löfberg, J. Guerrero Caballero, E. Bordes-Richard, A. Rubbens, R.-N. Vannier, H. Boukhlouf, A. Barama, Sol–gel synthesis and characterization of silica supported nickel ferrite catalysts for dry reforming of methane, Catal. Commun. 58 (2015) 127-131.

[36] Y.-H. Huang, S.-F. Wang, A.-P. Tsai, S. Kameoka, Reduction behaviors and catalytic properties for methanol steam reforming of Cu-based spinel compounds CuX_2O_4 (X=Fe, Mn, Al, La), Ceram. Int. 40 (2014) 4541-4551.

[37] A. Zarei Senseni, S.M. Seyed Fattahi, M. Rezaei, F. Meshkani, A comparative study of experimental investigation and response surface optimization of steam reforming of glycerol over nickel nano-catalysts, Int. J. Hydrogen Energy. 41 (2016) 10178-10192.

[38] J. Zhang, J.-M. Song, H.-L. Niu, C.-J. Mao, S.-Y. Zhang, Y.-H. Shen, $ZnFe_2O_4$ nanoparticles: Synthesis, characterization, and enhanced gas sensing property for acetone, Sensors Actuators B: Chem. 221 (2015) 55-62.

[39] L. Dong, C. Wu, H. Ling, J. Shi, P.T. Williams, J. Huang, Promoting hydrogen production and minimizing catalyst deactivation from the pyrolysis-catalytic steam reforming of biomass on nanosized NiZnAlOx catalysts, Fuel 188 (2017) 610-620.

[40] A. Vita, C. Italiano, C. Fabiano, L. Pino, M. Laganà, V. Recupero, Hydrogen-rich gas production by steam reforming of n-dodecane, Appl. Catal. B: Environ. 199 (2016) 350-360.

[41] S.A. Theofanidis, R. Batchu, V.V. Galvita, H. Poelman, G.B. Marin, Carbon gasification from Fe-Ni catalysts after methane dry reforming, Appl. Catal. B: Environ. 185 (2016) 42-55.

[42] D. Tian, Z. Liu, D. Li, H. Shi, W. Pan, Y. Cheng, Bimetallic Ni–Fe total-methanation catalyst for the production of substitute natural gas under high pressure, Fuel 104 (2013) 224-229.

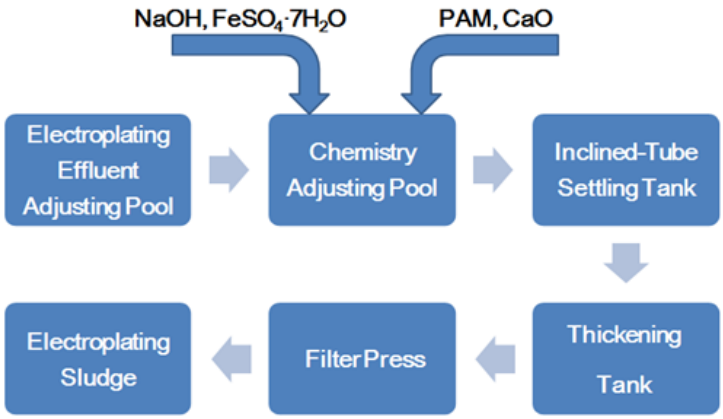

Fig. 1. The treatment process of electroplating wastewater to sludge (PMA: Polyscrylamide)

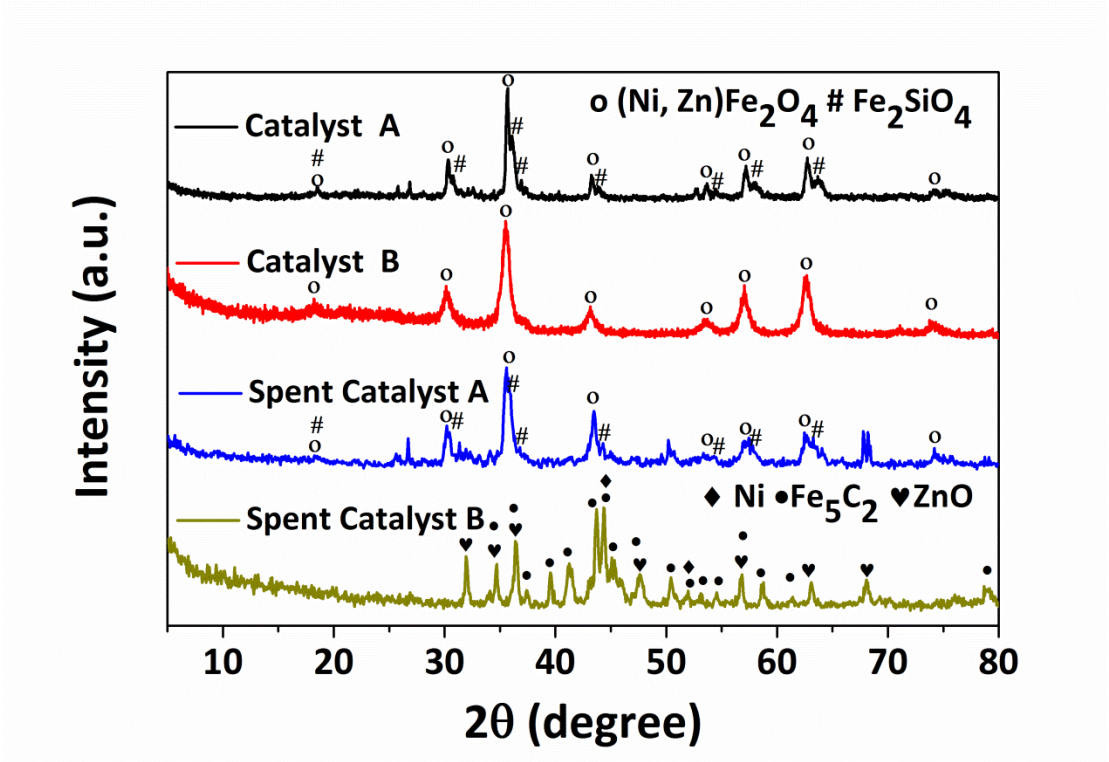

Fig. 2. XRD patterns of samples: Catalyst A, the ferrite sample prepared by sludge; Catalyst B, the ferrite sample prepared from chemical regents; Spent Catalyst A, the spent ferrite sample prepared by sludge; Spent Catalyst B, the spent ferrite sample prepared from chemical regents.

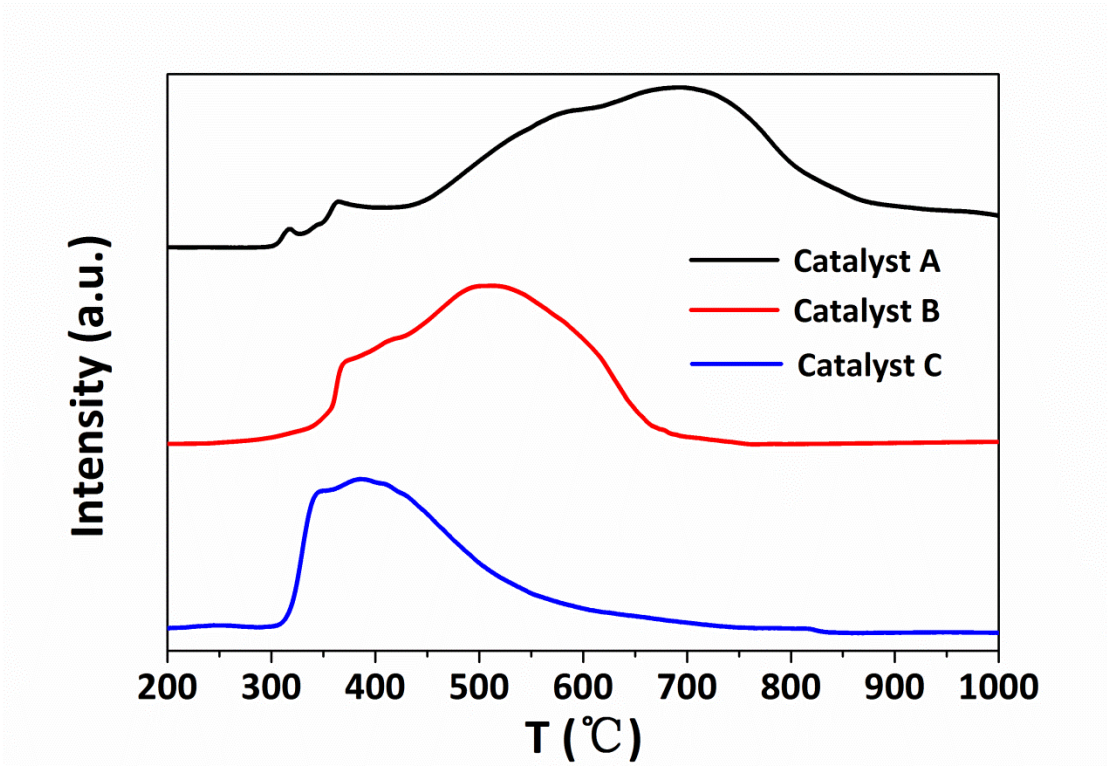

Fig. 3. H_2-TPR curves of samples: Catalyst A, the ferrite sample prepared by sludge; Catalyst B, the ferrite sample prepared from chemical regents; Catalyst C, sample J101 purchased from Nanjing Chemical Catalyst factory.

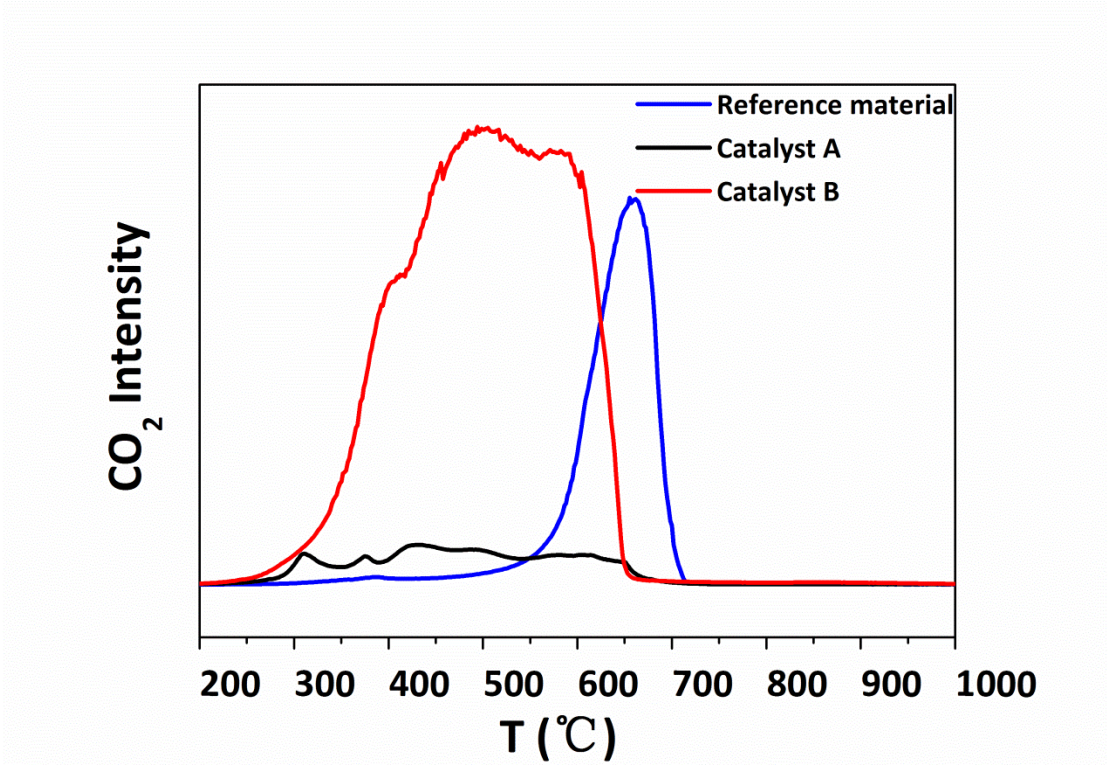

Fig. 4. O_2-TPO profile: CO_2 intensity as a function of temperature for used ferrite sample prepared by sludge (Catalyst A), used ferrite sample prepared from chemical regents (Catalyst B) and carbon black (Reference material). Heating rate of 10 $^{o}C \cdot min^{-1}$.

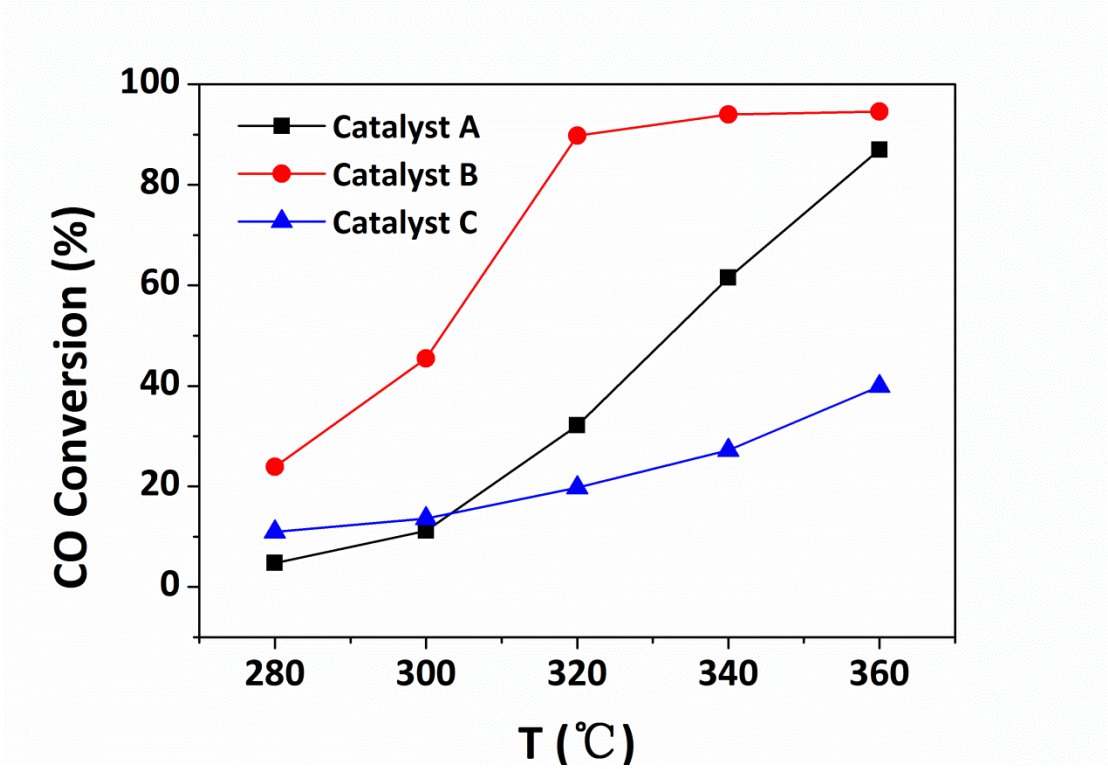

Fig. 5. The conversion of CO with the rising of temperature during methanation reaction. Reaction conditions: 2.0MPa, H_2/CO = 2. Catalyst A: the ferrite sample prepared from sludge; Catalyst B: the ferrite sample prepared from chemical regents; Catalyst C: sample J101 purchased from Nanjing Chemical Catalyst factory.

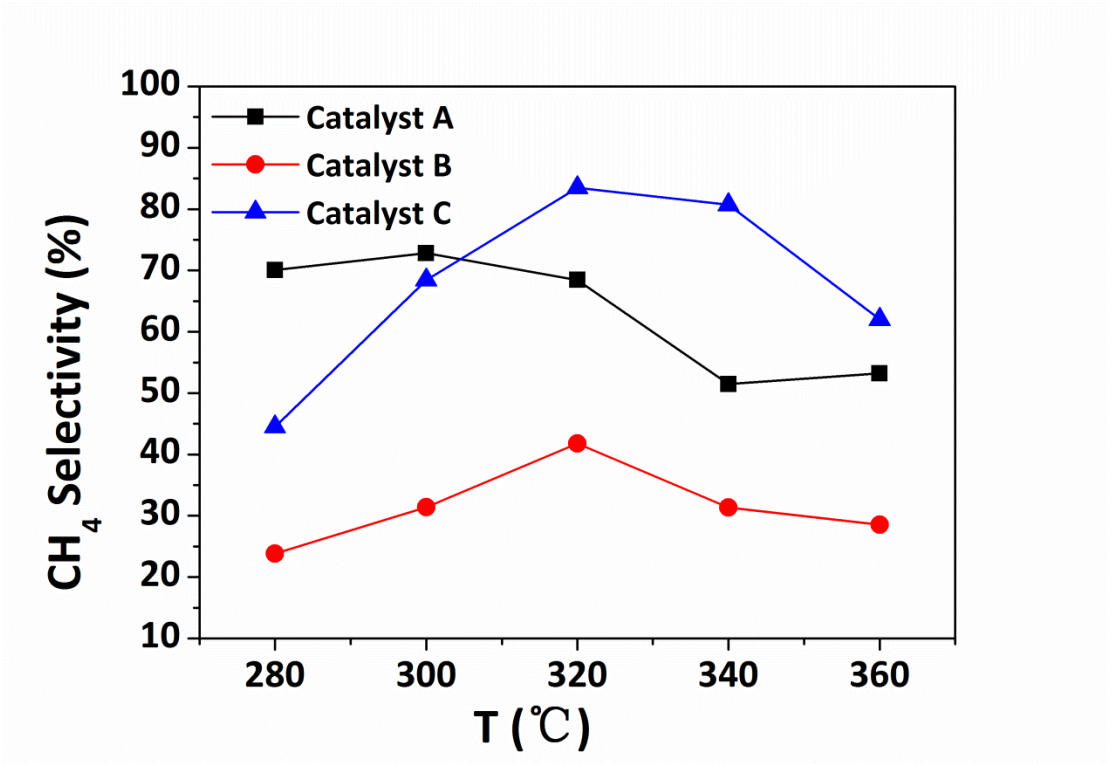

Fig. 6. The selectivity of CH_4 with the rising of temperature during methanation reaction. Reaction conditions: 2.0MPa, $H_2/CO = 2$. Catalyst A: the ferrite sample prepared from sludge; Catalyst B: the ferrite sample prepared from chemical regents; Catalyst C: sample J101 purchased from Nanjing Chemical Catalyst factory.

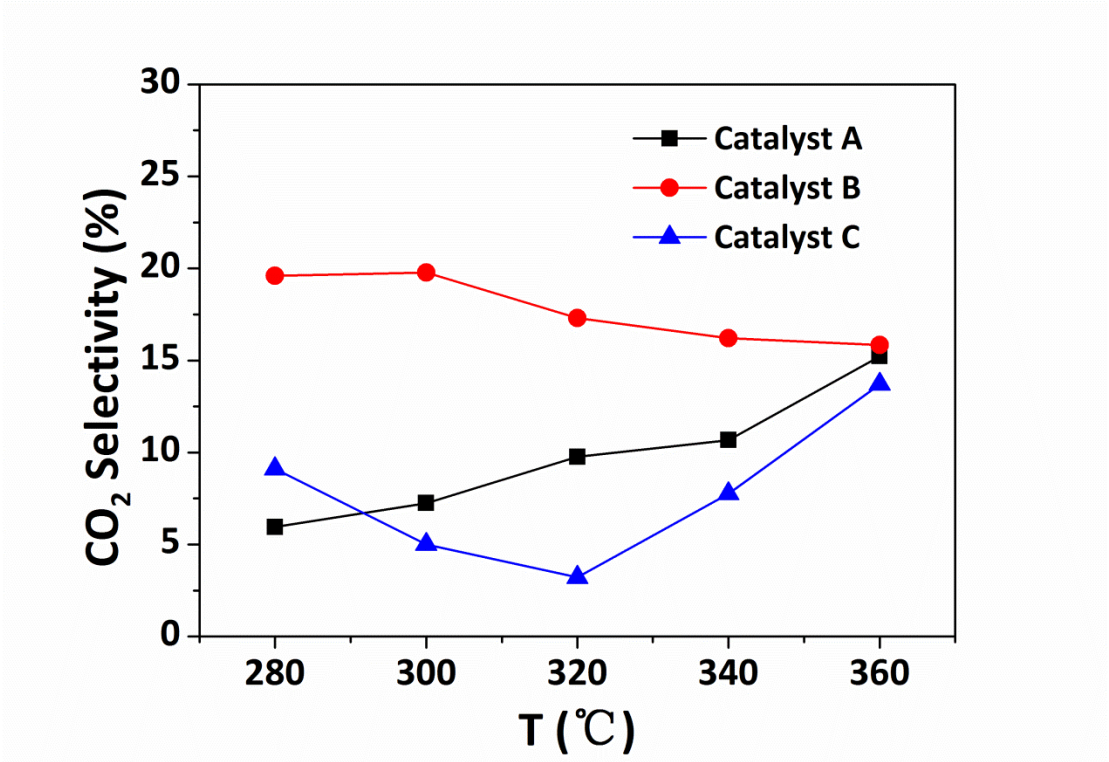

Fig. 7. The selectivity of CO_2 with the rising of temperature during methanation reaction. Reaction conditions: 2.0MPa, $H_2/CO = 2$. Catalyst A: the ferrite sample prepared from sludge; Catalyst B: the ferrite sample prepared from chemical regents; Catalyst C: sample J101 purchased from Nanjing Chemical Catalyst factory.

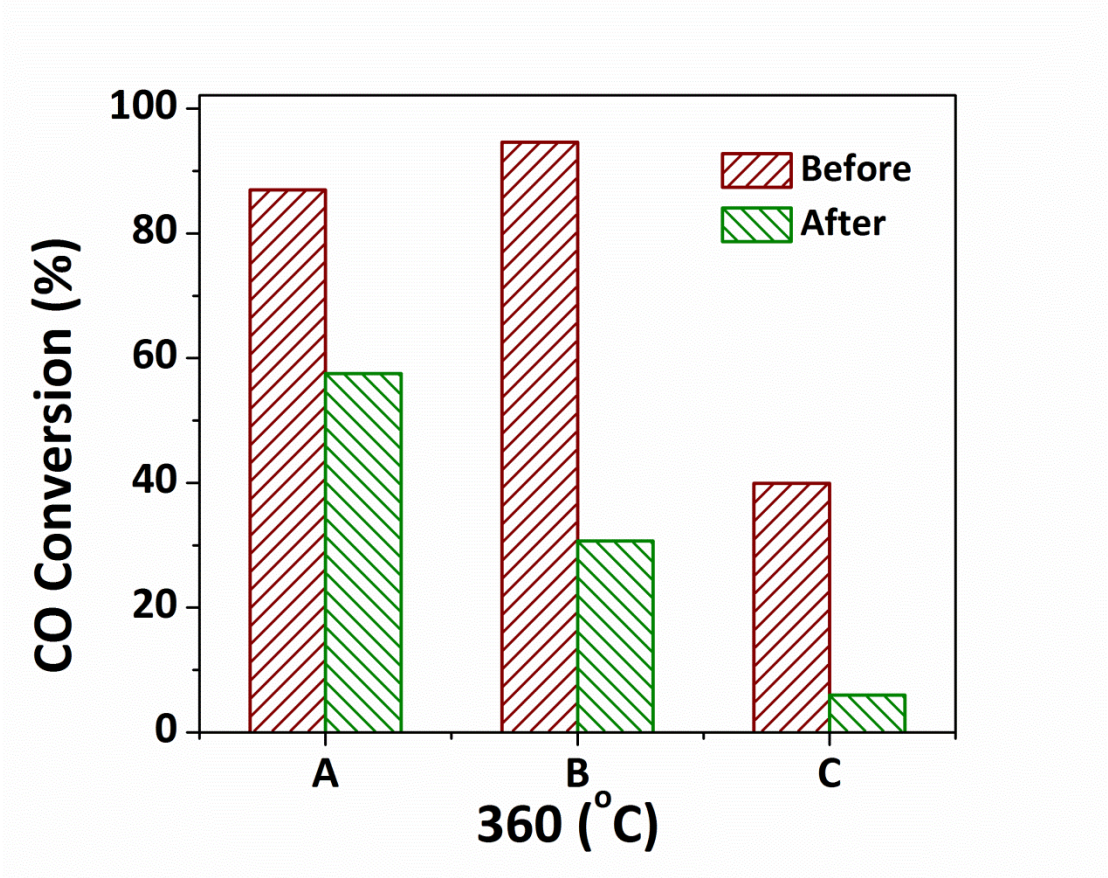

Fig. 8. The conversion of CO before and after the high-temperature processing: Catalyst A, the ferrite sample prepared from sludge; Catalyst B, the ferrite sample prepared from chemical regents; Catalyst C, sample J101 purchased from Nanjing Chemical Catalyst factory. Reaction conditions: 360 ^{o}C, 2.0MPa, H_2/CO = 2

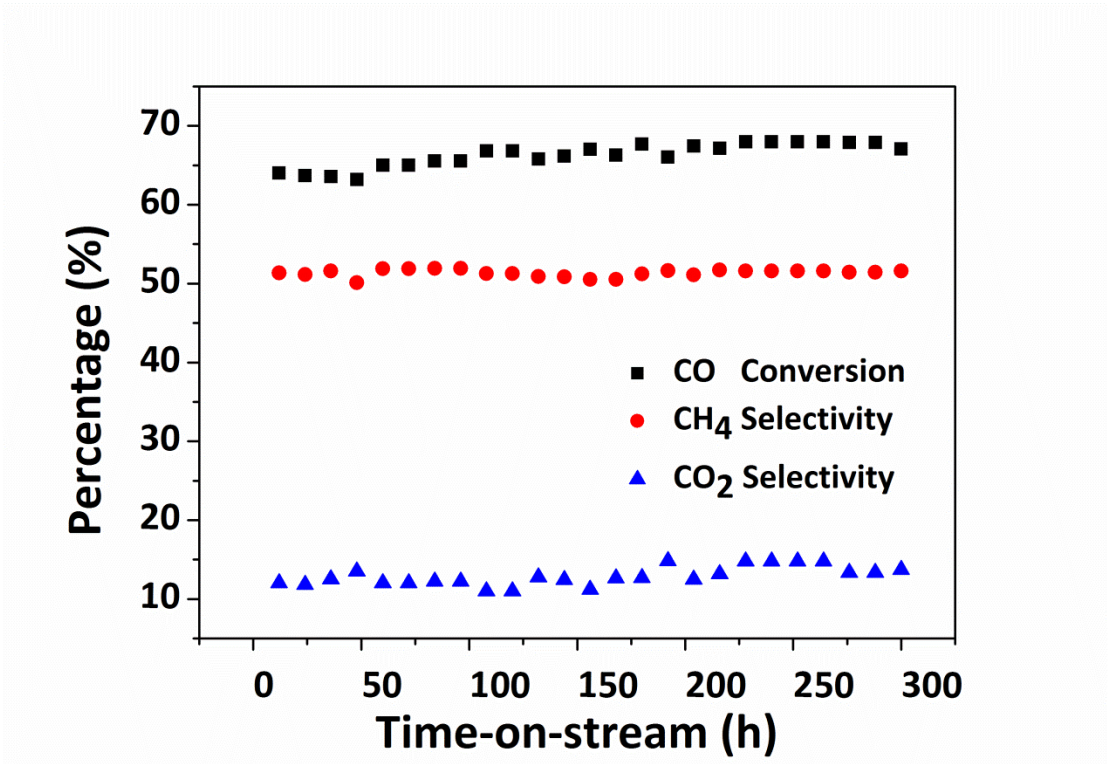

Fig. 9. Stability test of Catalyst A : ferrite sample prepared from sludge. Reaction conditions: 340 ^{o}C, 2.0MPa, H_2/CO = 2.

Table 1

Element contents of heavy metals in sludge

Samples	Elements							
	Zn	Ni	Fe	Cu	Cd	Al	Cr	Mn
Sample ^{S1} (wt%)	22.2	7.0	7.1	4.8	0.6	2.5	2.5	0.7
Sample ^{S2} (wt%)	1.8	0.8	23.9	3.1	0.7	5.0	2.1	0.5

Sample ^{S1}: Electroplating sludge from process S1

Sample ^{S2}: Electroplating sludge from process S2

Table 2

Textural properties and element contents of heavy metals of catalysts

Samples	Pore Size (nm)	Pore Volume ($cm^3 \cdot g^{-1}$)	Surface Area ($m^2 \cdot g^{-1}$)	Elements						
				Zn	Ni	Fe	Cu	Al	Cr	Mn
Catalyst A (wt%)	11.9	0.04	12.9	10.4	5.8	23.5	6.8	2.5	1.4	0.3
Catalyst B (wt%)	14.4	0.02	5.8	11.0	6.8	31.8	0	0	0	0
Catalyst C (wt%)	7.2	0.5	243.7	0	21.0	0	0	23.3	0	0

Catalyst A: The ferrite sample prepared by sludge.

Catalyst B: The ferrite sample prepared from chemical regents.

Catalyst C: Catalyst J101 purchased from Nanjing Chemical Catalyst factory.

.

Table 3

Product distributions of catalysts in methanation reactions

Catalyst	Q (MJ·N m^{-3})	CO conv. (%)	Selectivity (%)								
			CH_4	C_2H_6	C_2H_4	C_3H_8	C_3H_6	C_4H_{10}	C_4H_8	C_{5+}	CO_2
A	41.7	61.5	63.5	11.7	0.2	6.0	0.6	2.1	0.1	1.4	14.4
B	37.4	91.6	48.1	16.0	0	6.0	0	1.7	0	1.0	27.0
C	38.8	19.7	88.7	4.0	0.1	1.1	0.8	0.3	0.1	0.3	4.5

Reaction condition：Catalyst A was performed at 340 ^{o}C, Catalyst B was at 320 ^{o}C, Catalyst C was at 320 ^{o}C.

Table 4

Total manufactured cost of catalyst A, B and C.

Item/catalysts	A	B	C
Desalted water ($t \cdot t^{-1}$)	41.9	33.5	_
Desalted water cost ($\$ \cdot t^{-1}$)	106.7	85.3	_
Electroplating sludge (t)	1.8	_	_
Electroplating sludge Treatment cost ($\$ \cdot t^{-1}$)	-404.4	_	_
Electricity ($\$ \cdot t^{-1}$)	1004.3	803.7	_
Chemicals ($\$ \cdot t^{-1}$)	_	16074.9	_
Operating labors cost ($\$ \cdot t^{-1}$)	53.9	53.9	_
Depreciation ($\$ \cdot t^{-1}$)	149.8	149.8	_
Total costs ($\$ \cdot t^{-1}$)	910.3	17167.6	29962.6

[a] Dealing electroplating sludge spend 224.72 $\$ \cdot t^{-1}$. Thus feedstock of Catalyst A was assumed to be -224.72 $\$ \cdot t^{-1}$.

[b] The cost of electricity was calculated at 0.12 $/kw·h.